iScience

CellPress
OPEN ACCESS

Article

Emergence of complex oscillatory dynamics in the neuronal networks with long activity time of inhibitory synapses

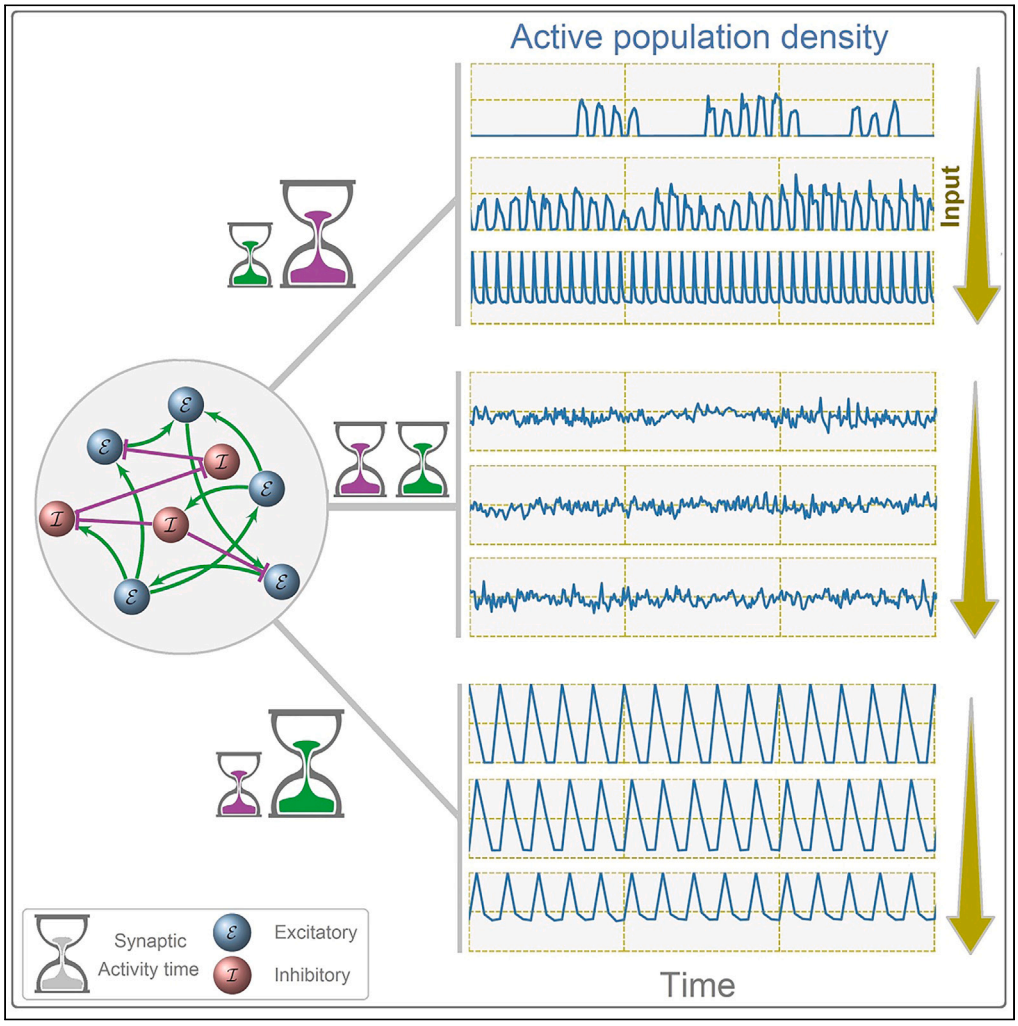

Mozhgan Khanjanianpak, Nahid Azimi-Tafreshi, Alireza Valizadeh

valizade@iasbs.ac.ir

Highlights

Simple models of excitable neurons reproduce complex neuronal collective dynamics

Brain's complex oscillations depend on prolonged activity of inhibitory synapses

Broad-band slow oscillations arise from the variability of the fast oscillations

Khanjanianpak et al., iScience 27, 109401
April 19, 2024
https://doi.org/10.1016/j.isci.2024.109401

iScience

CellPress
OPEN ACCESS

Article

Emergence of complex oscillatory dynamics in the neuronal networks with long activity time of inhibitory synapses

Mozhgan Khanjanianpak,[1,2] Nahid Azimi-Tafreshi,[1] and Alireza Valizadeh[1,2,3,*]

SUMMARY

The brain displays complex dynamics, including collective oscillations, and extensive research has been conducted to understand their generation. However, our understanding of how biological constraints influence these oscillations is incomplete. This study investigates the essential properties of neuronal networks needed to generate oscillations resembling those in the brain. A simple discrete-time model of interconnected excitable elements is developed, capable of closely resembling the complex oscillations observed in biological neural networks. In the model, synaptic connections remain active for a duration exceeding individual neuron activity. We show that the inhibitory synapses must exhibit longer activity than excitatory synapses to produce a diverse range of the dynamical states, including biologically plausible oscillations. Upon meeting this condition, the transition between different dynamical states can be controlled by external stochastic input to the neurons. The study provides a comprehensive explanation for the emergence of distinct dynamical states in neural networks based on specific parameters.

INTRODUCTION

The brain is a system of nonlinear components connected through a complex network and is considered as one of the most complex systems in the universe.[1] A variety of the nontrivial emergent phenomena that are widely studied in physical sciences are observed in brain dynamics, including synchrony,[2,3] multistability,[4,5] and criticality.[6–11] Brain oscillations, observed in a wide range of frequencies, emerge due to intricate interactions between the activities of the neurons in the local or distant regions.[12,13] The spectral pattern of the oscillations depends on the state of the brain and the region under study,[12] and the growing bunch of evidence support the crucial role of the oscillations in a variety of high level brain functions, such as attention,[14,15] perception,[16] memory,[17–19] and motor functions.[20,21] Therefore, a change in the properties of the oscillation patterns could indicate a malfunction in the brain in a causal way.[2,22–24] Theoretical studies have revealed different roles of the synchrony and the collective oscillations in the brain networks.[25–28] It is well known that while synchrony reduces the information capacity of an isolated system, in a distributed dynamical system with a modular structure like the brain it can facilitate the transmission of information and maximize mutual information between different functional modules.[29–31] Coordinated activity of the neurons produces stronger signals from the sources from one side[32,33] and modulates the excitability of the receiver networks on the other side, therefore providing a possible tool for control of the flexible communication between the brain areas.[34,35] This communication is crucial for the integration of the information processed in the functionally specialized brain regions that are essential for high level brain functions.[36–39] While biologically inspired conductance-based neuronal models are commonly used to study the dynamics of neural populations,[40–44] simpler models at different levels of abstraction are also employed to gain insight into the collective dynamics of neural populations.[45,46] These models are computationally efficient and allow for the study of fundamental rules underlying highly complex dynamics in the brain and other complex systems.[45,47–49] While networks composed of discrete time excitable components can reproduce oscillatory dynamics, they do not fully capture the properties of biological brain oscillations. In particular, gamma oscillations, which are generated by local populations of excitatory and inhibitory networks,[36,50,51] exhibit bursts of highly variable amplitude and period, interspersed with periods of low synchrony activity.[52,53] Additionally, gamma oscillations are nested within low frequency oscillations that modulate their amplitude.[54,55] These observations show that the collective brain oscillations produced by neurons differ from the periodic oscillations observed in many physical and biological systems, where coupled limit-cycle oscillators are common.[56,57] In the cortical networks of the brain, the balance between excitation and inhibition[58,59] results in neurons receiving a stochastic input with low mean and high variance. As a result, individual neurons fire sparsely and irregularly, despite the observed order in the macroscopic scale.[60] This highly variable amplitude and frequency, multi-frequency oscillation, and irregular dynamics of individual neurons have not been observed in simple computational models of brain networks. In this study, we aim to address this gap by developing a simple mathematical model that meets the minimum requirements for generating gamma oscillations with properties similar to

[1]Physics Department, Institute for Advanced Studies in Basic Sciences (IASBS), Zanjan 45137-66731, Iran
[2]Pasargad Institute for Advanced Innovative Solutions (PIAIS), Tehran 1991633357, Iran
[3]Lead contact
*Correspondence: valizade@iasbs.ac.ir
https://doi.org/10.1016/j.isci.2024.109401

those observed in the brain. Specifically, we sought to answer the question: "What properties of neuronal networks are necessary for the generation of biological gamma oscillations?" We hypothesized that incorporating synaptic dynamics, which was missing in previous studies using discrete models, is a crucial requirement for a valid neuronal model capable of reproducing biologically plausible oscillatory dynamics. Our findings demonstrate that by including synaptic dynamics in networks of excitable neuronal models, the network exhibits a variety of dynamical regimes similar to those observed in biological neural networks. To validate the model, we demonstrated its capability to generate spontaneously emerging oscillations with basic properties compatible with those of biological oscillations. Consistent with previous studies using spiking neural networks, we found that the duration of inhibitory synaptic activity is a crucial parameter that determines the properties of the oscillations. However, we discovered that biological oscillations only occurred when the inhibitory synapses had longer activity compared to the excitatory synapses. This constraint, which has been widely considered as a biological fact in computational studies, was not previously acknowledged for its critical importance in the emergence of complex neural dynamics.[61–63] Additionally, we demonstrated that when this criterion is met, the external stochastic input acts as a control parameter that governs the transition between different dynamical regimes resembling various states in the dynamics of the biological brain. Our findings also indicate that the intermittent dynamics of gamma oscillations observed at low levels of external input result in a broadband low-frequency component in the network's spectrum, which is generically coupled to the amplitude of the fast (gamma) oscillations. Our model consisted of the excitatory and inhibitory neurons where both types were implemented by an excitable model. The main advancement of the model compared to previous discrete time models was that the dynamics of synapses incorporated in the model were similar to the susceptible-infected-susceptible (SIS) epidemic models.[64] A synapse became active if its pre-synaptic neuron was active at the previous step and it remains active for a constant time that was chosen based on the observed values in realistic brain networks. The paper is divided into several sections. We begin by defining our model on a random network and examining the dynamics that influence the nodes and links. In Section Results, we present the results of our numerical simulations, exploring the influence of two control parameters, i.e., the noise strength and the time constant of the synapses, on the emergence of different activity patterns. Finally, we conclude the article in Section Discussion.

The model

The network

We consider a network of size N composed of 80% excitatory nodes (neurons) and 20% inhibitory ones. A pre-synaptic excitatory (inhibitory) node is connected to a post-synaptic node through an excitatory (inhibitory) directed connection. We denote excitatory (inhibitory) nodes with $\mathcal{E}$ ($\mathcal{I}$), such that $N_{\mathcal{E}} = 0.8N$ and $N_{\mathcal{I}} = N - N_{\mathcal{E}}$ indicate the number of $\mathcal{E}$ and $\mathcal{I}$ nodes, respectively. Similarly, the excitatory and inhibitory synapses are presented with E and I links, respectively. Both types of nodes are supposed to be connected randomly with a constant probability of p, such that each $\mathcal{E}$ ($\mathcal{I}$) node is connected through E (I) links to the other nodes. We also assume that all links have the same coupling strength. Figure 1A shows a schematic of the interaction network.

We define A as the adjacency matrix, such that for excitatory nodes $1 \leq j \leq N_{\mathcal{E}}$ (inhibitory nodes $N_{\mathcal{E}} < j \leq N$), $A_{ij} = 1$ if there is an excitatory (inhibitory) link from j to i and otherwise, $A_{ij} = 0$. We notice that there is no self-connection (autapse) in the network such that $A_{ii} = 0$ for all the nodes. Therefore, we can write the in-degree k_{in} and out-degree k_{out} of the nodes as follows:

$$k_{in}^{i} = k_{in}^{i,\mathbb{E}} + k_{in}^{i,\mathbb{I}} = \sum_{j=1}^{N_{\mathcal{E}}} A_{ij} + \sum_{j=N_{\mathcal{E}}+1}^{N} A_{ij} \quad \text{(Equation 1)}$$

$$k_{out}^{i,\mathbb{E}} = \sum_{j=1}^{N} A_{ji}, 1 \leq i \leq N_{\mathcal{E}} \quad \text{(Equation 2)}$$

$$k_{out}^{i,\mathbb{I}} = \sum_{j=1}^{N} A_{ji}, N_{\mathcal{E}}+1 \leq i \leq N \quad \text{(Equation 3)}$$

where $k_{in/out}^{i,\alpha}$ with $\alpha \in \{\mathbb{E}, \mathbb{I}\}$ indicates the number of incoming/outgoing links of type α for node i. All the outgoing links of excitatory (inhibitory) nodes are of excitatory (inhibitory) type, regardless of the type of target node. Figure 1B represents a schematic of the adjacency matrix composed of four blocks, where diagonal blocks indicate links between the nodes of the same type, while anti-diagonal ones represent connections between nodes of different types.

Dynamics of the nodes and the links

Compatible with realistic neurons, we assume that the nodes are excitable dynamical systems, which means that they remain inactive when stimulated weakly. However, when the stimulus exceeds a certain threshold, the neurons become active and generate a response. To model the dynamics of neurons in the network, we assign the activity state $\pi_i^{\alpha}(t)$ to each node i of α type ($\alpha \in \{\mathcal{E}, \mathcal{I}\}$) at each time t, such that when the neuron is activated $\pi_i^{\alpha}(t) = 1$, and otherwise $\pi_i^{\alpha}(t) = 0$. The binary state of the neurons is governed by a threshold condition, where the neuron's activation status changes based on this condition. Specifically, at each time step, if the internal inputs to a neuron reach a threshold value, it becomes activated. Conversely, if the threshold is not met, the neuron remains at rest. In the nervous system, the postsynaptic ion channels remain activated with a time constant that spans a wide range from a few to hundreds of milliseconds. To incorporate this fact in our

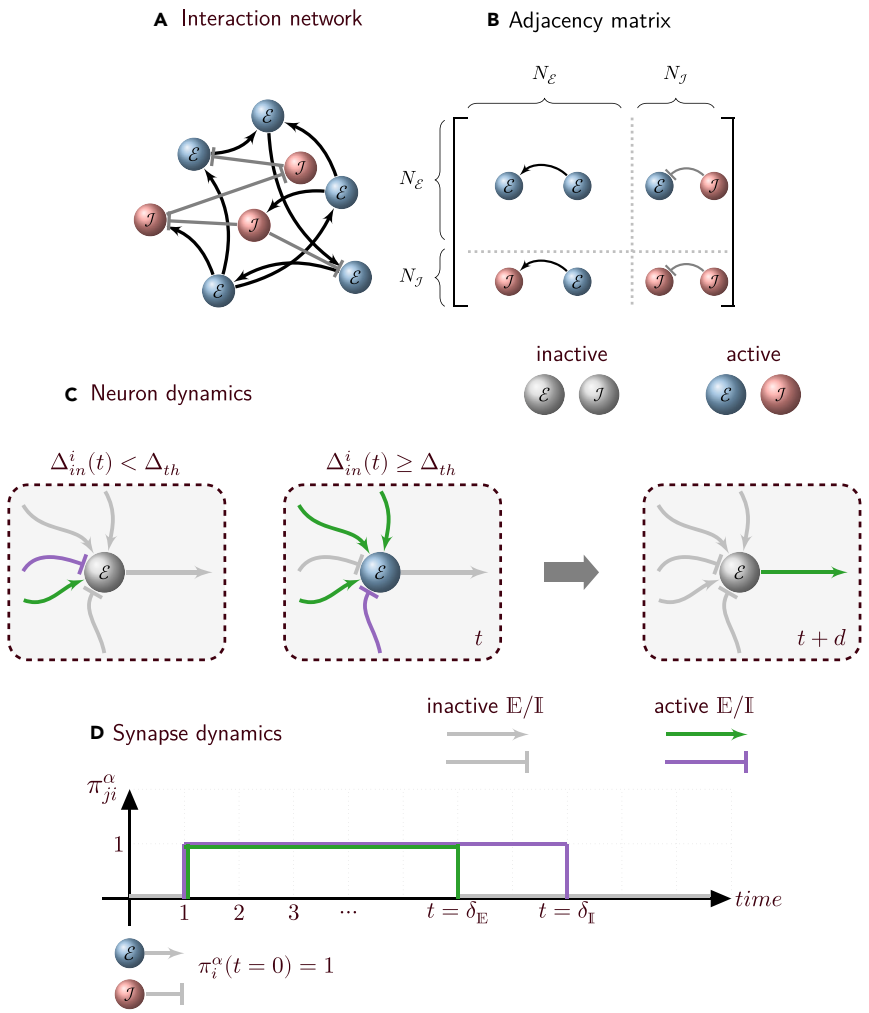

Figure 1. Connectivity network and the dynamics of the neurons and synapses

(A) Schematic representation of the network comprising excitatory ($\mathcal{E}$) and inhibitory ($\mathcal{I}$) nodes connected through a random connectivity matrix. Excitatory (E) and inhibitory (I) links are shown with black and gray colors, respectively.

(B) Schematic of the corresponding adjacency matrix that consists of four blocks connecting different types of neurons.

(C) An active neuron is presented by a colored node while a gray node shows an inactive neuron. Green and violet arrows indicate the active excitatory and inhibitory synapses, respectively. If the total input current Δ_{in} of a neuron is less than threshold Δ_{th}, it remains inactive, otherwise it gets activated (fires). All outgoing synapses of a firing neuron at time t become active after a delay of d at time $t+d$.

(D) The state of links as a function of time. If a pre-synaptic neuron is activated at $t = 0$, its outgoing links become active at $t = d$. A link of the type α remains active for δ_{α} time steps, and then the link is inactivated.

model, we assign a state to the links in the network that depends on the state of the presynaptic node as follows. When a neuron fires, all of its outgoing links become active after a synaptic delay time d and remain active for a time constant δ_{α} where α denotes the type of link (excitatory or inhibitory). To simplify our model, we make the assumption that the delay time for all links is uniform. Without loss of generality, we set the delay time $d = 1$. This allows us to scale other time constants relative to the delay. The synapse activity time constant, denoted as δ_{α}, varies depending on the type of synapse and is treated as a variable in this study. We denote the activity state of α type links, connecting node i to j, by $\pi^{\alpha}_{ji}(t)$ ($\alpha \in \{\mathbb{E},\mathbb{I}\}$). Each active $\mathbb{E}$ ($\mathbb{I}$) link exerts a positive (negative) current to the postsynaptic node. To replicate the balanced state observed in cortical networks, we set the magnitude of the excitatory current to unity. In contrast, the inhibitory currents are set to be four times stronger. This adjustment ensures that the inhibitory currents exhibit a greater strength relative to the excitatory currents, thereby mimicking the balanced state in cortical networks.[58] Therefore, The activity of neuron i at time t is determined by the total input current it receives, denoted as $\Delta^i_{in}(t)$. This input current is the sum of all excitatory and inhibitory currents. If the total input surpasses a specific threshold, the neuron becomes active. Otherwise, falling below the threshold, the neuron remains inactive:

- if $\Delta^i_{in}(t) < \Delta_{th}$ then $\pi^{\alpha}_i(t) = 0$ (inactive).

Table 1. Definition of the model parameters

Parameter	Definition	Parameter	Definition
$\mathcal{E}$	excitatory neuron	$\mathcal{I}$	inhibitory neuron
$\mathbb{E}$	excitatory synapse	$\mathbb{I}$	inhibitory synapse
N	total number of neurons	L	total number of synapses
A	adjacency matrix	δ_α	activity time constant of α type synapse
k_{in}^{α}	number of in-coming α type synapses	k_{out}^{α}	number of out-going α type synapses
η	noise probability intensity	d	synaptic delay time
Δ_{th}	membrane potential threshold	$\Delta_{in}^{i}(t)$	input current of neuron i at time t
π_i^{α}	activity state of α type neuron i	π_{ij}^{α}	activity state of α type synapse connecting neuron j to i
$\rho(t)$	density of active neurons at time t	$\varphi(t)$	density of active synapses at time t

- if $\Delta_{in}^{i}(t) \geq \Delta_{th}$ then $\pi_i^{\alpha}(t) = 1$ (active) and $\pi_{ji}^{\alpha}(t+1) = A_{ji}$,

where Δ_{th} is the threshold for the activation of the neurons. Figure 1C schematically shows the dynamics of the nodes and the links based on the sum of active links. As we already mentioned, when a node becomes active, its outgoing links become active after a delay time d and remain active for the time constant δ_α. Therefore, the post-synaptic node receives current during the time δ_α after a single activity of the pre-synaptic (see Figure 1D). To activate the network, all nodes receive an external noise in addition to the synaptic current they receive from other neurons in the network. This external noise represents the input from other parts of the nervous system. To this end, at each time step a fraction η of the $\mathcal{E}$ and $\mathcal{I}$ nodes fire randomly. To find the density of active nodes for both types ($\mathcal{E}$ and $\mathcal{I}$) as a function of time, we need to calculate the total input (synaptic input from the other nodes in the network and the external noise) to each node. We note that at each time step, for all pre-synaptic nodes j if $\pi_{ij}^{\alpha}(t) = 1$, the post-synaptic node receives an amount of $+1$ and -4 units of current through excitatory and inhibitory links, respectively. To capture this point, we define a weight matrix W such that $W_{ij} = \pi_{ij}^{\mathcal{E}}$ when $1 \leq j \leq N_{\mathcal{E}}$, otherwise $W_{ij} = -4\pi_{ij}^{\mathcal{I}}$. Hence, we can write the intra-network synaptic input to each node as follows:

$$\Delta_{in}^{i}(t) = \sum_{j=1}^{N} W_{ij}(t), \qquad \text{(Equation 4)}$$

In addition, the neurons receive noise and fire with probability η regardless of the recurrent synaptic input. Now we define $\rho_\alpha(t)$ ($\alpha \in \{\mathcal{E},\mathcal{I}\}$) and $\varphi_\alpha(t)$ ($\alpha \in \{\mathbb{E},\mathbb{I}\}$) as the fraction of active nodes and active links of α type at time t, respectively. Therefore, by summing up the state of nodes and links at t, we obtain the total fraction of active nodes $\rho(t)$ and links $\varphi(t)$ as follows:

$$\rho(t) = \rho_{\mathcal{E}}(t) + \rho_{\mathcal{I}}(t) = \frac{1}{N}\left(\sum_{i=1}^{N_{\mathcal{E}}} \pi_i^{\mathcal{E}}(t) + \sum_{i=N_{\mathcal{E}}+1}^{N} \pi_i^{\mathcal{I}}(t)\right) \qquad \text{(Equation 5)}$$

$$\varphi(t) = \varphi_{\mathbb{E}}(t) + \varphi_{\mathbb{I}}(t) = \frac{1}{L}\sum_{i=1}^{N}\left(\sum_{j=1}^{N_{\mathcal{E}}} \pi_{ij}^{\mathbb{E}}(t) + \sum_{j=N_{\mathcal{E}}+1}^{N} \pi_{ij}^{\mathbb{I}}(t)\right) \qquad \text{(Equation 6)}$$

where $L = \sum_{i,j}^{N} A_{ij}$ indicates the total number of links. A summary of model parameters is represented in Table 1.

RESULTS

We perform numerically simulations on a network with $N = 5000$, consisting $N_{\mathcal{E}} = 4000$ excitatory and $N_{\mathcal{I}} = 1000$ inhibitory neurons. We consider the interaction graph as an Erdős–Rényi (ER) random network, wherein $\mathcal{E}$ and $\mathcal{I}$ nodes are connected with a probability of $p = 0.1$, regardless of the type of nodes. Therefore, mean in-degree is $\langle k_{in}\rangle \simeq pN = 500$ where the mean number of incoming E and I links are 400 and 100, respectively. The mean out-degree of the excitatory and inhibitory nodes is $\langle k_{out}^{\mathbb{E}}\rangle = \langle k_{out}^{\mathbb{I}}\rangle \simeq 500$. When a node becomes active at time t, the outgoing links of node becomes active after delay time at $t+d$, and post-synaptic nodes receive an input that lasts for $\delta_{\mathbb{E}}$ and $\delta_{\mathbb{I}}$ time steps for the E and I links, respectively. The nodes, whose input current exceeds the threshold value, become active at the same time and spike. We set the threshold value $\Delta_{th} = 4$. Simulations are run for $t_{max} = 25000$ time steps.

Emergence of oscillations in the network

To demonstrate the mechanism of the generation of collective oscillations in the network, we have shown the dynamics of the network in Figure 2, for an exemplar set of the parameters. We set external input to all the nodes, such that on average regardless of the recurrent synaptic inputs and the neurons type, a fraction $\eta = 0.001$ of the neurons fire randomly at each time step. This is compatible with the brain networks where every population that represents a region of the brain, continuously receives external input from the other parts of the brain. We

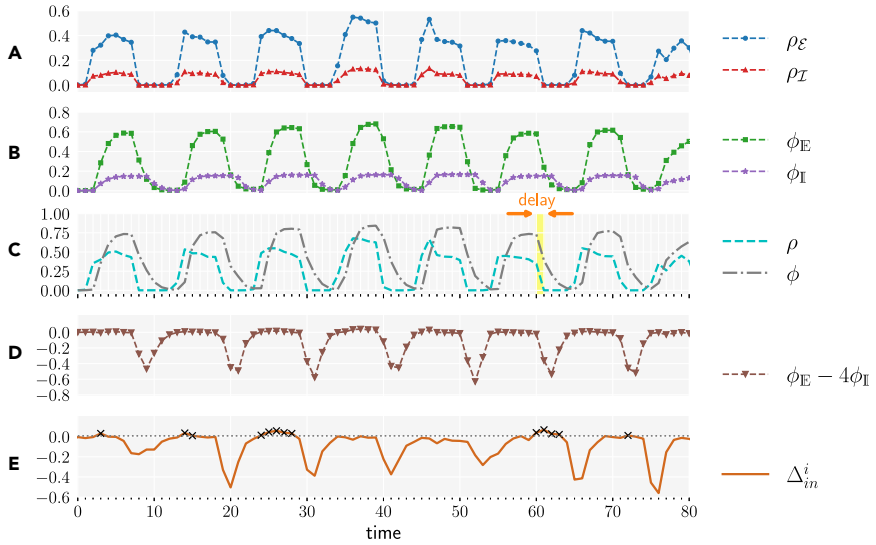

Figure 2. Emergence of the oscillatory dynamics

(A) Fraction of active excitatory nodes $\rho_{\mathcal{E}}$ (blue dots) and inhibitory nodes $\rho_{\mathcal{I}}$ (red triangles) and (B) fraction of active excitatory links $\varphi_{\mathbb{E}}$ (green squares) and inhibitory links $\varphi_{\mathbb{I}}$ (violet stars) versus time t.

(C) Fraction of total active nodes ρ (dashed line) and active links φ (dotted-dashed line) versus time t.

(D) Mean input current in the network and (E) normalized input current of a random node versus time t. The dotted horizontal line denotes normalized threshold Δ_{th} and the black cross mark symbols represent times in which the neuron fires. Note the irregular firing of the neuron despite the collective oscillations. The results are obtained on ER network with $N = 5000$, $\langle k_{in}^{\mathbb{E}} \rangle = 400$ and $\langle k_{in}^{\mathbb{I}} \rangle = 100$, wherein 80% of neurons are excitatory. Other parameters are $\eta = 0.001$, $\delta_{\mathbb{E}} = 5$, $\delta_{\mathbb{I}} = 7$, and $\Delta_{th} = 4$. The synaptic current of inhibitory links is 4 times greater than the excitatory ones.

See also Figure S1.

also take $\delta_{\mathbb{E}} < \delta_{\mathbb{I}}$, which is an important criterion, as will be revealed later. Figure 2A shows the time course of the fraction of active E and I neurons. It is observed that the behavior of $\rho_{\mathcal{E}}(t)$ and $\rho_{\mathcal{I}}(t)$ is similar and both show oscillations with variable time courses in different cycles. The time course of the fraction of active $\mathbb{E}$ and $\mathbb{I}$ links are also shown in Figure 2B. Similar to the nodes, the fraction of active links oscillates in time in a sustained way, but with variable time courses during different cycles. Notably, I links stay active for a longer time compared to E links since $\delta_{\mathbb{I}} > \delta_{\mathbb{E}}$. For a better comparison, we have also shown the time course of the density of all the active (sum of the excitatory and inhibitory) neurons $\rho(t)$ and active links $\varphi(t)$, in Figure 2C. The activity of the links follows that of the nodes with a time lag $d = 1$, as we expect. In addition, the maximum value of φ is always greater than ρ (see section Dynamic details about the activation of nodes and links; Figure S1 for more details). Assuming all the links are inactive, applying noise causes some random excitatory and inhibitory nodes to fire. Therefore, about $\eta N \langle k_{out} \rangle$ synapses will be activated at the next time step, of which %80 are excitatory, and the rest are inhibitory. This recurrent synaptic input increases the probability of the firing of the neurons that receive excitatory inputs, and more neurons are recruited by the active population. Due to the high out-degree of the neurons, the whole network receives the recurrent inputs after one or two time steps and the activity of the network rapidly increases. Since inhibitory synapses are four times stronger than the excitatory ones, $\varphi_{\mathbb{E}} - 4\varphi_{\mathbb{I}}$ gives the average synaptic input current to the neurons in the entire network. It is notable that despite the increase in the density of active synapses, the average value of $\varphi_{\mathbb{E}} - 4\varphi_{\mathbb{I}}$ remains around zero (see Figure 2D), as a result of dynamical balance in the network.[58,59] Although the average input is almost zero, individual neurons can receive net supra-threshold current and become activated, as is shown in Figure 2E. Later in the time course of a cycle, the fraction of active nodes and links starts to decrease since $\delta_{\mathbb{E}} < \delta_{\mathbb{I}}$. Hence $\varphi_{\mathbb{E}}$ decreases faster than $\varphi_{\mathbb{I}}$ and the inhibitory input of neurons considerably exceeds the excitation. Therefore, the chance of firing of the neurons dramatically decreases, which leads to the cease of the activity of the network (see Figures 2C and 2D). The next cycle begins when the average input to the neurons approaches zero, and some neurons in the network again can fire due to external input and supra-threshold input to the random individual nodes. Note that the spiking activity of the neurons is irregular, and a representative neuron might fire multiple times or not fire in different periods of network oscillation (Figure 2E).

Effect of external input: Types of activity patterns

As discussed in the previous section, the external input plays a major role in the dynamics of the network by activating a small fraction of the neurons whose activity spreads in the network and initiates different cycles (see Sec. Introduction). Here, we investigate how the level of the external input can lead to the activation of different numbers of neurons and drive the network to different dynamic states. We performed the simulations wherein the fraction of externally activated nodes η changes in the interval between (0,1), while all other parameters are kept fixed. Figure 3A shows $\rho(t)$ over a 700 time steps for different values of η (increasing level of the external input) from top to bottom.

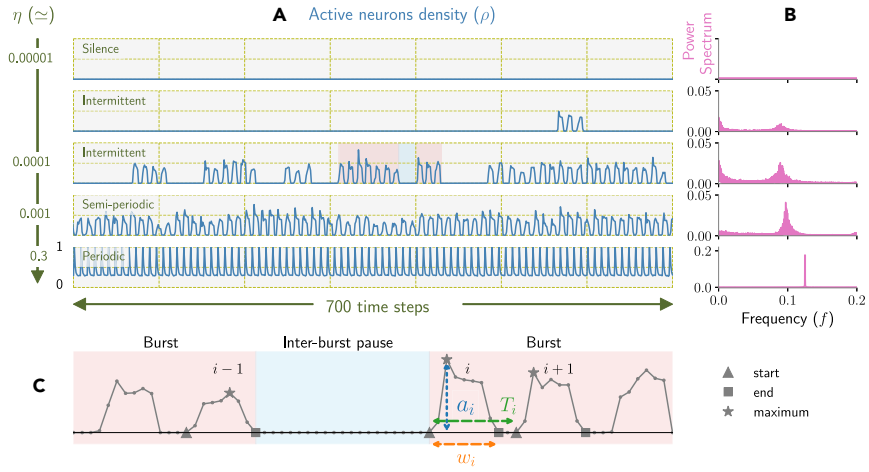

Figure 3. Different activity regimes

(A) The fraction of active neurons $\rho(t)$ in 700 time steps. From top to bottom, the noise intensity η increases which results in the emergence of four phases; silence, intermittent, semi-periodic, and periodic. Parameters are set as $\delta_{\mathbb{E}} = 5$, $\delta_{\mathbb{I}} = 7$, and $\Delta_{th} = 4$.

(B) The power spectrum of the network activity for the four phases shown in (A).

(C) Time course of ρ where two bursts and one inter-burst interval are highlighted with red and blue. The triangles, stars and squares indicate the start point, the maximum value and the endpoint of each cycle, respectively. a_i specifies the amplitude, w_i is the duration, and T_i is the period of the ith activity.

See also Figure S2.

When the external input is very small, the intensity of excitation is not enough to exploit more neurons and to initiate an activity cycle and the network effectively remains in a "silence" phase. In this phase, only a few neurons randomly activate in each time step due to the external input.

As the excitation input to the network increases, higher proportion of externally activated nodes rises the probability of the initiating an activity cycle. These activity cycles typically appear in the bursts of activity each consisting of several cycles, similar to the bursts of spontaneous gamma oscillations in the brain.[52,65–67] Bursts (a collection of activity peaks) appear randomly and are separated by "inter-burst pauses (IBPs)", over which the activity is very low $\rho(t) \approx 0$. We call this regime of the activity an "intermittent" phase. For the lower values of η, the bursts are separated by long inter-burst pauses and increasing the external input shortens the pauses and increases the duration of the bursts (Figure 3A, second and third rows). This intermittent behavior manifests itself in the power spectrum as the appearance of a peak in high frequencies, representing intra-burst fast oscillatory activity, and a broad peak in low frequencies representing inter-burst statistic that is the appearance of the bursts in random, with a long timescale compared to intra-burst dynamics (Figure 3B, second and third rows). For $\eta \simeq 10^{-3}$, the inter-burst interval approaches zero and bursts merge. This "semi-periodic" phase is characterized by the cycles of activity with variable amplitude and time courses, as was shown in Figure 2. In this regime low-frequency peak in the spectrum, representing inter-burst dynamics vanishes. It is also notable that intra-burst frequency remains constant with increasing the external input and the period of the oscillations within the bursts is not affected by the input in this range (Figures 3A and 3B, fourth row). Further increasing the input enhances the regularity of the oscillations. In this phase, the amplitude of peaks is precisely the same and equal to the maximum value of $\rho(t) = 1$, and the spectrum shows a pronounced peak indicating a regular "periodic" phase (Figures 3A and 3B, last row). In the periodic regime, the minimum activity of the network, troughs of the oscillations, increases with the higher inputs, such that ultimately at $\eta = 1$ all the neurons remain active i.e., $\rho(t) = 1$ at all the time steps, as expected.

To better explore the different phases, we have shown the statistic of the bursts in the intermittent regime in Figure 4 and those of the cycles in three different states in Figure 5. The distribution of the duration of the bursts and the pauses shown for three different values of the noise in Figure 4 confirm the presence of the long IBPs for weak noises, and long bursts for strong ones. In both cases, the long tail of the distributions suggests that the start and end of the bursts are the result of a stochastic process, which is further explained in section Dynamic details about the activation of nodes and links (see Figure S1). These results show that the duration and the rate of the generation of the bursts are highly dependent on the strength of the external noise. To explore the statistics of the cycles, we define attributes of period T_i, amplitude a_i, and duration w_i for each activity cycle as demonstrated in Figure 3C. Distribution of these three measures during the oscillatory behavior in the periodic, semi-periodic, and within the bursts in the intermittent phase is shown in Figure 5. Notably, the distributions shown in the first two rows of Figure 5, indicate that the intra-burst oscillatory dynamics are quite similar to that of the semi-periodic state. Increasing the noise in this range does not impact the properties of the cycles within the bursts and only alters the rate and the duration of the bursts (Figure 4). These two states, intermittent and semi-periodic, are both characterized by the variability in the amplitude and the period of the oscillations' cycles. This variability in the oscillatory activity decreases with further increasing the external input, leading to periodic dynamics observed in the lowest row of Figure 3A and the third row of Figure 5. As shown in Figure 3B, our findings indicate that the wax and wane of high frequency oscillations during the intermittent state contribute to the presence of a broadband peak in low frequencies. In contrast, previous studies have

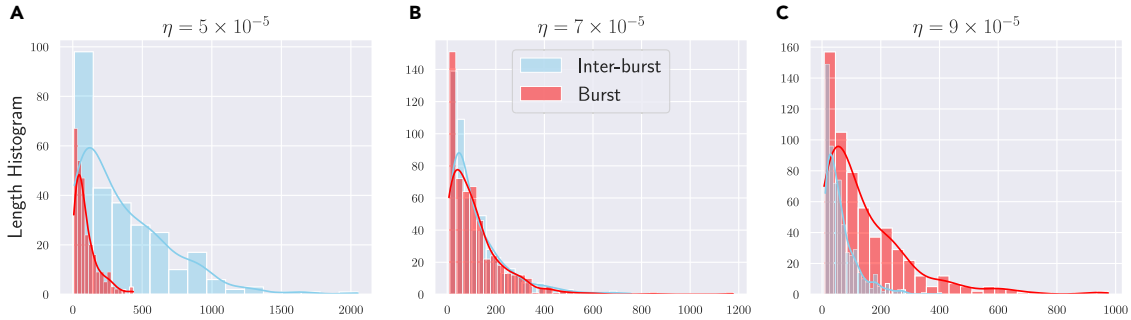

Figure 4. Statistics of activity bursts in the intermittent phase

Distribution of duration of the bursts (red) and the inter-burst pauses (blue) in the intermittent phase with $\delta_{\mathbb{E}} = 5$ and $\delta_{\mathbb{I}} = 7$. The intensity of the applied noise is increased from (A)–(C) as indicated on the top of each panel. The results are averaged over 10 realizations.

proposed that other mechanisms such as adaptation or short term synaptic plasticity that operate in slower time scales, typically several hundreds of milliseconds, underlie the generation of slow rhythms.[68–71] In the other words, the slow and fast oscillations observed in these studies are generated by distinct mechanisms. Notably, our model lacks such distinct mechanisms with slow time scales and slow spectral components are an emergent dynamical phenomenon resulted from the intermittent appearance of the bursts of the fast oscillations. Therefore, the peak in the low frequencies in our model is only seen in the intermittent state (see the second and third rows of Figure 3B). Moreover, in our model the relationship between the phase of slow oscillations (SOP) and the amplitude of the fast oscillations (FOA) is generic since the slow oscillations are a result of the variable amplitude fast oscillations and they are not generated by a different mechanism. To show the relationship between fast and slow oscillations in our model, we first identified low and high frequency components in the time course and in the spectrum of the network activity in the intermittent state (Figures 6A and 6B). Then we showed the amplitude of the fast oscillations in different phases of the slow oscillations and the corresponding distribution of amplitudes in Figures 6C and 6D, respectively. Non-uniform distribution of the FOA with respect to the SOP is an indicator of the non-zero phase-amplitude coupling (PAC).[54,72–74] We also show the dependency of FOA and SOP for a broad range of external noise between $10^{-5} \leq \eta \leq 10^{-4}$, in which intermittent phase is observed, in Figure 6E. Notably, coupling between the fast and slow oscillations is detectable for the whole range of intermittent phase.

Effect of synaptic time constants

In the above simulations, we assumed that the activity time of the inhibitory links is greater than the excitatory ones, i.e., $\delta_{\mathbb{I}} > \delta_{\mathbb{E}}$, compatible with the typical values of the time constants of fast receptors of AMPA and $GABA_A$.[75] For comparison, it is important to test the results for other cases when the activity time of the excitatory synapses is equal to, or larger than the inhibitory ones. For $\delta_{\mathbb{E}} = \delta_{\mathbb{I}}$, the density of active nodes behaves in a different way, and we observe another phase, namely noisy oscillations, where the network activity fluctuates around a mean value with small amplitude (see supplementary). Figure S2A shows that the behavior of $\rho(t)$ in this regime is almost independent of the noise amplitude η. For all the values of noise amplitude, a distinguished frequency is observed in the power spectrum and the peak's frequency does not change with noise (Figure S2B). This behavior is a consequence of the balance between mean excitation and inhibition at all the time steps so that only fluctuations in the net input can activate the nodes in the network. Furthermore, when $\delta_{\mathbb{E}} > \delta_{\mathbb{I}}$, (see Figures S2C and S2D) a periodic phase is observed for almost the whole range of the external input level except for the case that the noise intensity is too low. The difference between the behavior of the network with different relations between excitatory and inhibitory time constants is further explored by showing different collective dynamical attributes in the three cases. In Figure 7 we have shown the power spectrum, and in Figure 8, the period, the mean amplitude, and the mean density of the active neurons are shown in (a)-(c) versus η and for three different values of inhibitory time constant in (e)-(f) versus $\delta_{\mathbb{I}}$ for different values of noise. For $\delta_{\mathbb{E}} > \delta_{\mathbb{I}}$ periodic behavior with constant frequency (period) and amplitude is observed in all the range of the input, except for very small and very large values over which the system will be in the silence and in the fully active state, respectively. Spectrum has a single pronounced peak in the oscillation frequency with zero component over other frequencies (Figure 7A). Furthermore, over a wide range of input levels, the mean value of activity, the amplitude, and frequency of the oscillations are constant and independent of the input (Figures 8A–8C). On the other hand, the nonzero spectrum of the network activity over a wide frequency range (Figure 7B) indicates noisy oscillations for the case $\delta_{\mathbb{E}} = \delta_{\mathbb{I}}$, except for the extreme values of η that drive the network to silence and fully active states. As is seen in Figures 8A–8C, in this case, the mean value of the activity, the amplitude and the frequency of the oscillations are again independent of the input level over a wide range of η, and the amplitude is considerably smaller, compared to the case $\delta_{\mathbb{E}} > \delta_{\mathbb{I}}$. When $\delta_{\mathbb{E}} < \delta_{\mathbb{I}}$, the intermittent and the semi-periodic states are also recognizable as is shown in Figure 7C. For both states, the spectrum has components for all the frequencies reflecting the irregularity of the dynamics, whereas for the intermittent state a broad peak in low frequencies, reflecting the inter-burst statistics, is also apparent. Compared to noisy oscillations of the case $\delta_{\mathbb{E}} = \delta_{\mathbb{I}}$, here both the amplitude and the period of the oscillations are larger as seen in Figures 8A and 8B. Compatible with theoretical and simulation studies with conductance-based neuronal models, our results (Figures 7C and 8A) show that the frequency of the oscillations is not significantly affected by the input level.[56] The small amplitude of the oscillations in the intermittent and semi-periodic states (the square and triangle symbols in Figure 8B) is indicative of the

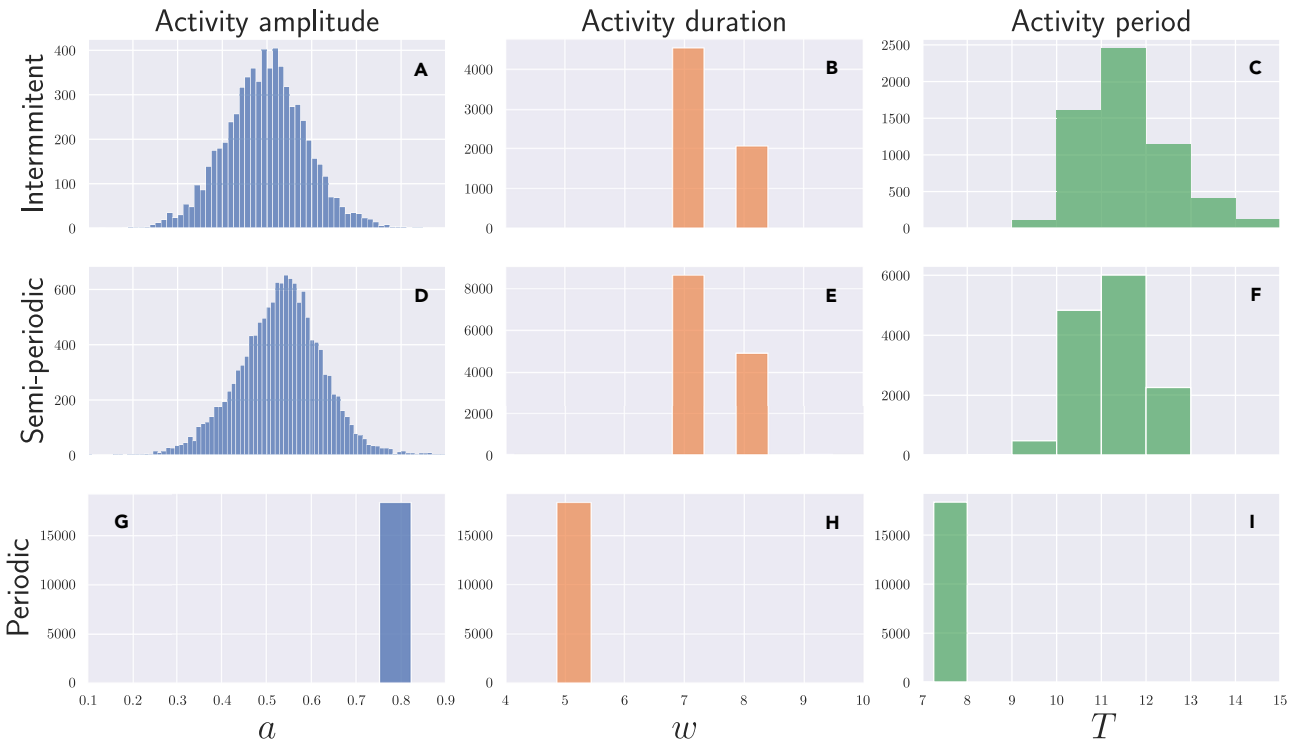

Figure 5. Analysis of the activity at different states

From left to right, histograms of amplitude, activity duration, and period respectively are shown for (A–C) intermittent, (D–F) semi-periodic and (G–I) periodic phases. Parameters are $\delta_{\mathbb{E}} = 5$, $\delta_{\mathbb{I}} = 7$, and $\Delta_{th} = 4$. The results are averaged over 10 realizations.

so-called sparse firing of the single neurons that are observed in the gamma oscillations.[56] In these states, the firing of the neurons is not regular despite oscillatory activity at the network level. The irregular firing of sample neurons in this state is shown in the supplementary (Figure S3). Notably, in the intermittent and semi-periodic regimen single neurons do not fire in every cycle of the oscillations and instead, over the time windows that the inhibition and excitation are almost balanced (i.e., inhibition is not dominant in the network), they randomly fire due to the random fluctuation of the single neurons input around zero. As noted above, the transition of the intermittent to semi-periodic state takes place through the expansion and the merge of the oscillation bursts, therefore, changing input in this range (from 10^{-5} to 10^{-2}) does not significantly affect the properties of the oscillations as is seen in Figures 8A and 8B. However, the emergence of the regular oscillations (at $\eta \simeq 10^{-2}$) is accompanied by a drop in the period and an increase in the amplitude of the oscillations right at the transition point. Moreover, Figure 8C indicates that the mean value of active neurons, $\langle \rho \rangle$, almost remains constant in the semi-periodic state, while rising in the intermittent and periodic states with increasing the input level. In Figures 8D–8F we have also shown the dependence of the mean activity value, the period and the amplitude of the oscillations to the inhibitory synaptic time constant. As is seen in Figure 8D the period of the oscillations increases with δ_I almost linearly, for different values of the input level. This is in accordance with the previous results observed in the EI networks composed of conductance-based model neurons.[56] Moreover, the amplitude of the oscillations clearly shows the difference in the results for three cases where δ_I is smaller than, equal to, or larger than δ_E. Notably, the small amplitude of the oscillations for very small δ_I (Figure 8E) is due to the nonzero activity in the troughs of the periodic oscillations. For $\delta_I = \delta_E$ small amplitude is a hallmark of the state of the noisy oscillations seen in Figure 7 and for $\delta_I > \delta_E$ oscillation amplitude depends on the input and resulting state of the network. Figure 8F also shows that in both cases $\delta_{\mathbb{I}} < \delta_{\mathbb{E}}$ and $\delta_{\mathbb{I}} > \delta_{\mathbb{E}}$, the mean value of active neurons decreases as the inhibition activity time increases.

The results presented in this section are summarized in Figure 9 where the dynamical state of the system is shown in the parameter space including external noise and the inhibitory time constant. It is seen that the switching between the states of neural networks and biologically relevant states of intermittent and semi-periodic oscillations with sparse firing of the single neurons is only observable when $\delta_{\mathbb{E}} < \delta_{\mathbb{I}}$. These results highlight the important role of the biological observation that inhibitory synapses typically decay in a relatively longer time compared to excitatory ones.[76–81] With this criterion, plausible oscillations can be expected from the neural networks compatible with those seen in the brain dynamics.

The validity of the results in more realistic models

Our model aimed to possess very basic properties of biological neural networks, leading to several structural and dynamical simplifications in its construction. In this section, we examine the robustness of the main results against exemplar changes in the network structure and

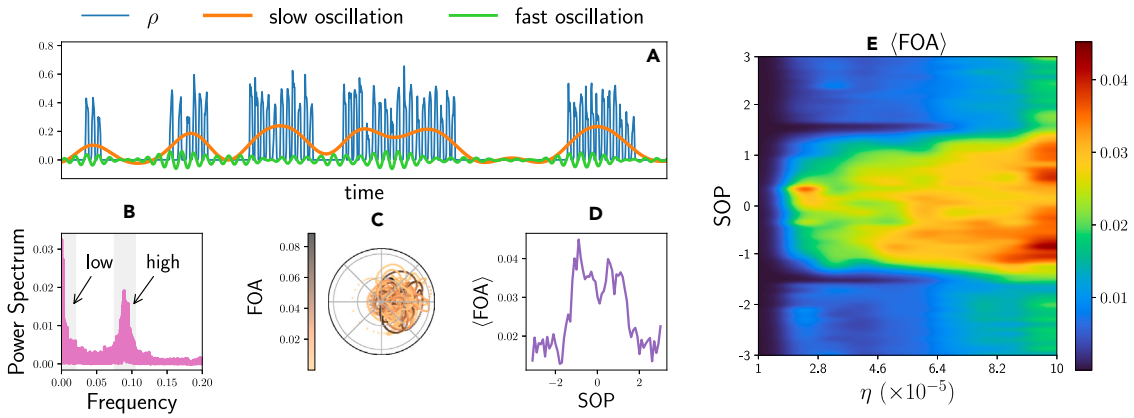

Figure 6. Phase amplitude coupling for the intermittent state

(A) The blue curve shows the fraction of active neurons $\rho(t)$ in a window of 1600 time steps when $\eta = 5 \times 10^{-5}$. The orange and green curves show the low and high-frequency components of ρ, whose frequency range is depicted by the shaded area in the power spectrum of the activity shown in panel (B). The amplitude of fast oscillation (FOA) at different phases of slow oscillation (SOP) is shown in panel (C). The non-uniform distribution of the mean amplitude of the fast oscillations over different phases of the slow oscillations (panel (D)) is a hallmark of the coupling between the two variables. Such coupling can be observed in a broad range of external noise η over which intermittent phase is observed, as is shown in panel (E).

model parameters that make the model more representative of a realistic brain network. In the first experiment, we altered the connectivity between the excitatory neurons. Previous experiments have indicated that the connectivity between excitatory neurons is sparser than other types of connections (see e.g.,[82]). While in the main experiments all connection types were assumed to have similar probabilities, here we reduced the probability of the $\mathcal{E} \to \mathcal{E}$ connections. The results shown in Figure S4 are qualitatively in line with those presented in Figure 3. All activity regimes are present in the new variant of the model, and the only change is that the domain of intermittent regime is smaller. Other properties of the model, including the frequency of the oscillations, remained unaltered compared to the main model with equal probabilities of connections. In the next variant, we tested how changes in the network's topology can affect the results. In the main model, we assumed that the network's connectivity is random (Figures 1A and 1B).[3,27,60,62,83–89] Although this topology is a good approximation for brain connectivity on small scales ($\lesssim$100 microns), it does not take into account the decrease in connection probability with distance,[82] or the presence of long-range connections between different regions.[90] To test how changes in topology affect the results and to incorporate long-range connections, we constructed a small-world network by rewiring the excitatory connections in a regular network (see Figures S5A and S5B, and STAR Methods).[91–98] The results shown in Figures S5C and S5D confirm that the primary findings with random networks remain applicable in this alternative topology, as all regimes (silent, intermittent, semi-periodic, and periodic) appear in the collective dynamics when changing the external drive. Another simplification in our model was that the inhibitory and excitatory conductance were assumed to maintain a constant value during synapse activity. However, after a typically sharp upraise, the conductance of biological synapses decays exponentially with a decay time constant that effectively specifies the duration of synapse activity. To incorporate this fact in our model, we considered an exponential decay for synaptic activity with the decay time, instead of synaptic activity time in previous sections (see STAR Methods). Figures S6 and S7 show different activity regimes on a random network for three cases of $\delta_{\mathbb{E}} < \delta_{\mathbb{I}}$, $\delta_{\mathbb{E}} = \delta_{\mathbb{I}}$, and $\delta_{\mathbb{E}} > \delta_{\mathbb{I}}$. Similar to Figure S2A, we observe noisy oscillations with a smaller frequency that are independent of noise amplitude when $\delta_{\mathbb{E}} = \delta_{\mathbb{I}}$. Furthermore, by comparing Figures S7C and S2C, for the whole range of external input level, only the periodic phase is detected in the case of $\delta_{\mathbb{E}} > \delta_{\mathbb{I}}$. Accordingly, just like the simple model, different states including intermittent and semi-periodic states are observed, as shown in Figure S6D, only when $\delta_{\mathbb{E}} < \delta_{\mathbb{I}}$. In summary, these experiments validate the main results of the manuscript using more biologically realistic models. These findings help identify fundamental properties of neurons and synaptic connections that contribute to the emergence of complex oscillations in the brain.

Dynamic details about the activation of nodes and links

In this section, we aim to explain how a sparse network consisting large number of neurons is activated by receiving a very small noise. Considering the interaction graph as an Erdős–Rényi (ER) random network with $N = 5000$ and $p = 0.1$, we set external input to all the nodes as $\eta = 0.001$ such that, on average, four excitatory and one inhibitory neurons fire randomly at each time step. Regarding Figure S1A, let us assume the neurons labeled with A to D and U are respectively the excitatory and inhibitory ones that fire at time $t = 0$. According to the model, all outgoing links of the active neurons become active after a synaptic delay time $d = 1$. Given the mean out-degree $\langle k^{\mathbb{E}}_{out} \rangle = \langle k^{\mathbb{I}}_{out} \rangle \simeq 500$, about $l_{\mathbb{E}} = 2000$ excitatory and $l_{\mathbb{I}} = 500$ inhibitory synapses become active at $t = 1$. Then with setting the threshold value $\Delta_{th} = 4$, all those neurons in the network that have in-going synapses from neuron A-D but not from neuron U, receive a minimum amount of input current to get activated (see nodes E and F in Figure S1B). The probability that we find such nodes is obtained by $P(t)$ which is derived by regarding the conditions for each time t. Deriving $P(t)$, about $NP(t)$ neurons will fire at each time t as a result of synaptic current. Moreover, $N\eta$ neurons fire

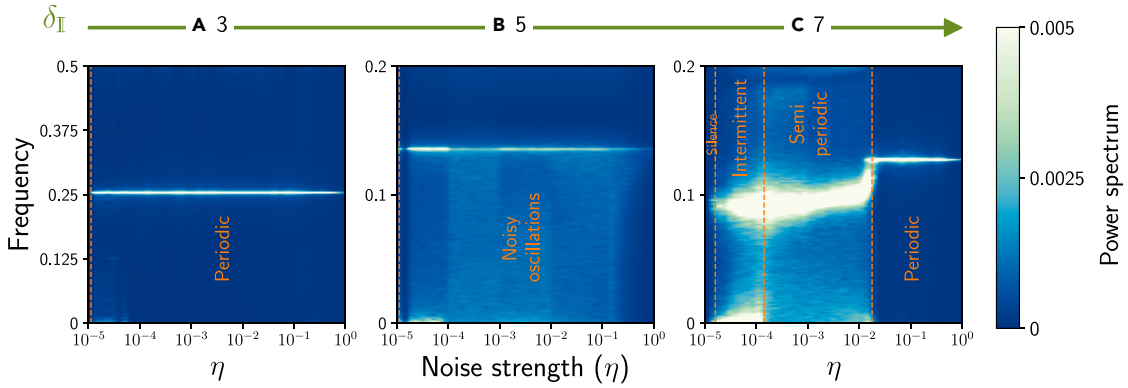

Figure 7. Spectral analysis of the different activity phases

Power spectrum of the density of active neurons versus noise intensity for different activity times of inhibitory synapses. The activation time of inhibitory synapses $\delta_{\mathbb{I}}$ is indicated on the top of panels (A)–(C), while $\delta_{\mathbb{E}} = 5$. Vertical dashed lines separate phases.

directly due to the noise (for example see nodes G-J and V in Figure S1B) although some of them may have been already activated because of synaptic current. Consequently, at most, $n_{\mathcal{E}}(t) = [P(t) + \eta]N_{\mathcal{E}}$ excitatory and $n_{\mathcal{I}}(t) = [P(t) + \eta]N_{\mathcal{I}}$ inhibitory neurons have the chance to fire at t. Here at $t = 1$, by employing binomial distribution we obtain $P = C_4^4 C_0^1 p^4(1 - p)$ where $C_b^a = \frac{a!}{b!(a-b)!}$. The number of active excitatory and inhibitory nods are also obtained as $n_{\mathcal{E}} = 1 + 4 = 5$ and $n_{\mathcal{I}} = 0 + 1 = 1$. To estimate the number of active links of type α at time t, we notice that the number of active nodes in the previous time steps is an important variable. Given the rules governing synapse dynamics, active links remain active for the time constant δ_α. Hence, we need to take into account the number of active nodes at previous time steps between $t - \delta_\alpha$ and $t - 1$. Therefore, we can estimate the maximum possible value of the α type active links as $l_\alpha(t) = \langle k_{out}^\alpha \rangle \sum_{i=1}^{\delta_\alpha} n_\alpha(t - i)$. Consequently, the fraction of active synapses of type α is always more than or equal to the active neurons fraction of that type: $\varphi_\alpha(t) = \frac{l_\alpha(t)}{L} \geq \rho_\alpha(t) = \frac{n_\alpha(t)}{N}$. We also notice that if at time t a node whose links are active fires (due to noise or synaptic current) it does not affect the number of active links at the next time step. Now according to the given description, we obtain $l_{\mathbb{E}} = 4500$ and $l_{\mathbb{I}} = 1000$ at $t = 2$. To estimate P at this time, we need to consider that there are $4 + 5 = 9$ excitatory and $1 + 1 = 2$ inhibitory nodes whose out-going links have been already activated. Based on the threshold value, only the following two types of neurons fire due to synaptic current:

- Nodes that have in-going links from at least four of nine $\mathcal{E}$ type nodes but not from the two inhibitory ones.
- Nodes that have in-going links from at least eight of nine excitatory nodes but from only one of the two $\mathcal{I}$ ones.

For the first and second items we obtain the probabilities $P_1 = \sum_{b=4}^{9} C_b^9 C_0^2 p^b (1 - p)^{11-b}$ and $P_2 = \sum_{b=8}^{9} C_b^9 C_1^2 p^{b+1} (1 - p)^{10-b}$, respectively. Hence, $(P_1 + P_2 + \eta)N_{\mathcal{E}}$ excitatory and $(P_1 + P_2 + \eta)N_{\mathcal{I}}$ inhibitory neurons fire at $t = 2$ (see Table S1). Similarly, we can proceed by estimation of the density of active nodes and links at each time t (Figure S1C). It is clear that in the interval between $t = 1$ to $t = \delta_{\mathbb{E}}$ the values of ρ and φ increase. However, passing through the activation time of excitatory synapses, the number of excitatory nodes whose out-going links are still active starts to fall. This results in a dramatic reduction in the number of active excitatory links, such that the net current within the network becomes substantially negative (see Figure 2D). Hence, the chance of firing due to synaptic current reduces and both ρ_α and φ_α start to decline. Notably, the number of neurons activated by noise is not big enough to increase ρ_α and φ_α dramatically. This reduction continues until passing activation time of inhibitory synapses. Then, repeating the scenario, oscillations are formed periodically.

DISCUSSION

The study of oscillatory dynamics and the role of these oscillations in high-level brain functions has long been a focal point in brain sciences.[12–15,27–31,34–36] Brain oscillations provide a mechanism for the efficient and flexible communication between the brain areas that is crucial for the high-level brain functions such as memory, perception, and motor functions.[14–21] Disruptions in the normal patterns of oscillations can impair proper communication in the brain and contribute to a variety of brain and cognitive disorders.[2,22–24] Neural oscillations arise from intricate interactions between neurons, which are mediated by a complex network of local and long-range synaptic connections.[2,12,56,88,99] Various neuronal and synaptic properties can influence the pattern of oscillatory activity in the brain by affecting the electrical activity of neurons and synaptic connections. Given the high-dimensional parameter space of neuronal populations and the multitude of factors that may contribute to the generation of oscillations, theoretical and simulation studies with simplified reduced models are essential for understanding the role of different physiological constraints in rhythm genesis in the brain. In this work, our aim was to introduce a computationally efficient discrete-time model that captures the essential aspects of biological neuronal networks, such as neuronal excitability and synaptic dynamics. While previous studies have utilized similar discrete neuronal models based on excitable components,[45,46,48,49] they have struggled to reproduce the complex dynamics observed in biological neural networks. We sought to determine the minimal requirements for constructing a simplified model capable of capturing neural oscillatory dynamics. This research has

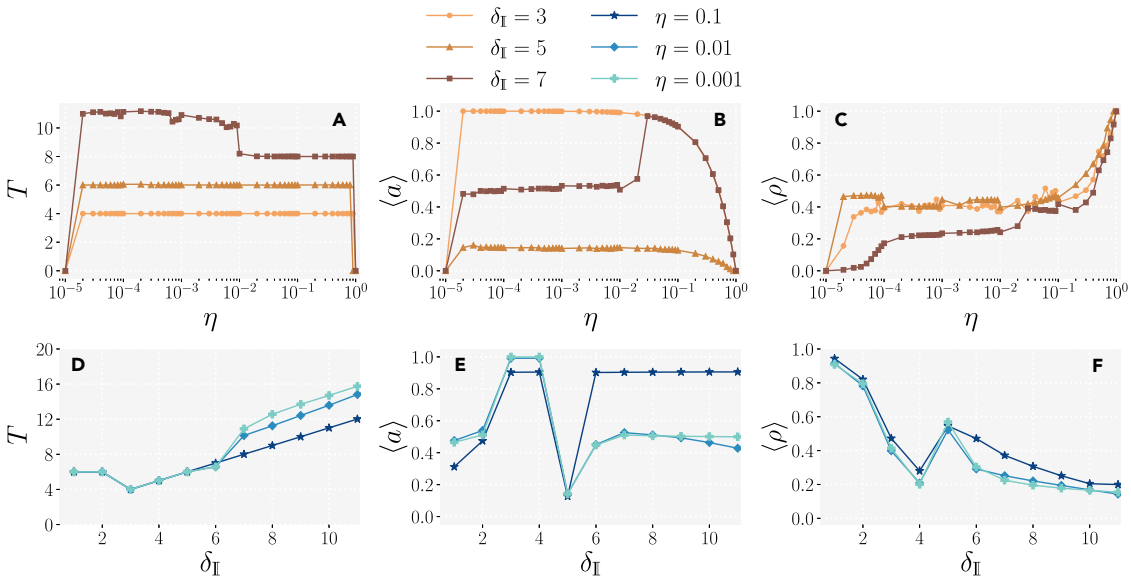

Figure 8. Effect of noise and inhibition activity time on the activity of the neurons

The period of activities, the mean amplitude of cycles and the mean value of active neurons, (A–C) versus noise intensity η for different values of $\delta_{\mathbb{I}}$ and (D–F) versus inhibition activity time $\delta_{\mathbb{I}}$ for different values of η. $\delta_{\mathbb{E}} = 5$ and the results are averaged over 10 realizations.

See also Figure S3.

two main benefits: it provides insights into the essential properties of neural networks that contribute to rhythm generation and other emergent collective states, and it establishes a lower limit on how much the model can be simplified and which properties can be discarded when designing a minimal model. Our study highlights the importance of incorporating synapses with prolonged activity as additional dynamical elements in the model to replicate the collective dynamics observed in biological neuronal networks. To evaluate the model's applicability, we incorporated several basic biological constraints commonly used in simulating cortical local networks, such as random connectivity, the fraction of excitatory and inhibitory neurons, and the balance between inhibition and excitation.[56] Our results demonstrate that despite its simplicity, the model can reproduce complex oscillations where the period of oscillations is determined by the activity time of inhibitory synapses. This finding is consistent with previous computational and theoretical studies on gamma-band oscillations.[29,36,56,57,88] In addition, we utilized the model to investigate the role of a commonly overlooked constraint in simulating cortical neural populations: the longer activity of inhibitory synapses compared to excitatory synapses. While recent studies have identified very fast and strong inhibitory connections in the hippocampus,[57,100] experimental evidence consistently supports the longer activity of GABA-A receptors compared to AMPA receptors. By incorporating this constraint into our model, we were able to explore the advantages of the slower activity of the GABA-A receptors and its impact on the dynamics of neural networks.[75,101,102] Our observations revealed that the emergence of different dynamical regimes and complex oscillations are critically dependent on this constraint. Specifically, we found that the longer activity of inhibitory synapses compared to excitatory synapses is responsible for the appearance of oscillations with variable amplitudes, and sparse firing of neurons within cycles, as well as the emergence of low-frequency broad-band oscillations that modulate the amplitude of faster oscillations. We demonstrated that removing this constraint eliminates some of the dynamical regimes in the phase diagram of the model, resulting in a considerably simpler collective activity that is incompatible with that observed in biological neuronal networks. Furthermore, our study revealed that external input serves as a control parameter that regulates the collective dynamics and transition of the network between various dynamical regimes. Importantly, the role of external input is only significant when the time constant of inhibitory links is greater than that of excitatory links. By varying the parameters of inhibitory time constants and noise levels, we constructed a phase diagram of the model and identified the range of parameters over which different states can be observed. In comparison to commonly used conductance-based models, our model offers significant computational advantages. This is because, in continuous time models, each millisecond is divided into multiple time steps, requiring numerous arithmetic operations at each step depending on the model's complexity.[103] In our model, each time step is approximately equivalent to the duration of an action potential, which is about one to two milliseconds. This significantly reduces computational costs, meanwhile, the simplicity of our model allows for a more comprehensible interpretation of the observed dynamics (Figure S1), facilitating the elucidation of principles governing different dynamical regimes in brain networks. In summary, we presented a neuronal network model based on the very fundamental properties of neurons and synapses: membrane excitability and prolonged synaptic activity. Our findings suggest that many features of the brain's complex dynamics emerge from the interaction of simple excitable neuronal models through non-instantaneous synapses in the network. Due to its simplicity, our model allows for a detailed examination of the mechanism underlying the emergence and disappearance of complex oscillations.

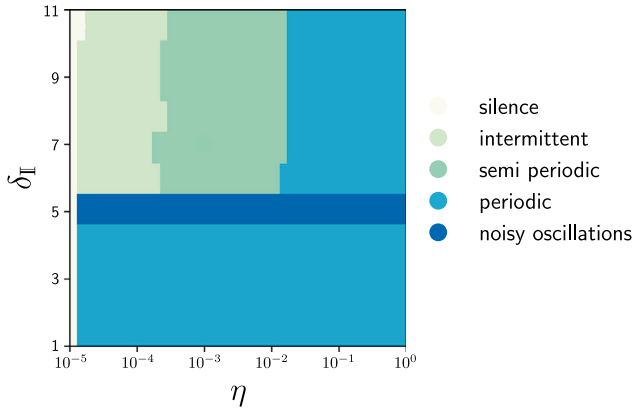

Figure 9. Phase diagram in the space $\eta - \delta_{\mathbb{I}}$

The phase diagram of the model as a function of noise η and time constant of inhibitory links $\delta_{\mathbb{I}}$ while $\delta_{\mathbb{E}} = 5$.

Limitations of the study

Achieving a balance between abstraction and biological realism in the neuronal models is a critical challenge for neuroscientists.[104,105] Biologically plausible neuronal models strive to closely mirror the physiological and anatomical characteristics of real neurons and neural circuits. These models incorporate a wealth of biological data, including ion channel kinetics, synaptic dynamics, and network connectivity patterns, to emulate the behavior of actual neurons.[106] While biologically plausible models offer a more faithful representation of neural processes, they often come with increased computational complexity and data requirements, making them less scalable for certain applications. Our study's model resides at the other end of the spectrum. Emphasizing simplicity and computational efficiency to capture essential neural and synaptic activity, we implemented a highly abstract neuronal model. While suitable for theoretical exploration and large-scale simulations, our model may overlook biological details and struggle to accurately replicate the complexities of real neural systems. Notably, our model lacks several characteristic properties of biological neurons, such as adaptation, bursting, and refractoriness.[103,104,107,108] Additionally, the biological synapses we used in the model are far less complex than their real counterparts, which exhibit a wide range of weights and time constants, and their efficacy can be altered through short- and long-term plasticity rules.[109,110] However, the model holds potential for incorporating more of these properties in future iterations. Furthermore, the study's predictions could be validated by utilizing models featuring biologically plausible spiking neuronal networks.

STAR★METHODS

Detailed methods are provided in the online version of this paper and include the following:

- KEY RESOURCES TABLE
- RESOURCE AVAILABILITY
  - Lead contact
  - Materials availability
  - Data and code availability
- METHOD DETAILS

SUPPLEMENTAL INFORMATION

Supplemental information can be found online at https://doi.org/10.1016/j.isci.2024.109401.

ACKNOWLEDGMENTS

No specific funding was received for conducting this study.

AUTHOR CONTRIBUTIONS

A.V. and M.K. conceived the study. M.K. performed the numerical analysis. N.A.-T. and M.K. wrote the original draft. A.V. edited the manuscript and wrote the final version.

DECLARATION OF INTERESTS

The authors declare no competing interests.

Received: June 12, 2023
Revised: December 30, 2023
Accepted: February 28, 2024
Published: March 4, 2024

REFERENCES

1. Eguiluz, V.M., Chialvo, D.R., Cecchi, G.A., Baliki, M., and Apkarian, A.V. (2005). Scale-free brain functional networks. Phys. Rev. Lett. *94*, 018102.
2. Buzsaki, G., and Draguhn, A. (2004). Neuronal oscillations in cortical networks. Science *304*, 1926–1929.
3. Wang, X.J. (2010). Neurophysiological and computational principles of cortical rhythms in cognition. Physiol. Rev. *90*, 1195–1268.
4. Kelso, J.A.S. (2012). Multistability and metastability: understanding dynamic coordination in the brain. Philos. Trans. R. Soc. Lond. B Biol. Sci. *367*, 906–918.
5. Madadi Asl, M., Valizadeh, A., and Tass, P.A. (2018). Dendritic and axonal propagation delays may shape neuronal networks with plastic synapses. Front. Physiol. *9*, 1849.
6. Shew, W.L., and Plenz, D. (2013). The functional benefits of criticality in the cortex. Neuroscientist *19*, 88–100.
7. Plenz, D., Ribeiro, T.L., Miller, S.R., Kells, P.A., Vakili, A., and Capek, E.L. (2021). Self-organized criticality in the brain. Front. Physiol. *9*, 639389.
8. Massobrio, P., de Arcangelis, L., Pasquale, V., Jensen, H.J., and Plenz, D. (2015). Criticality as a signature of healthy neural systems. Front. Syst. Neurosci. *9*, 22.
9. Beggs, J.M., and Timme, N. (2012). Being critical of criticality in the brain. Front. Physiol. *3*, 163.
10. Beggs, J.M. (2008). The criticality hypothesis: how local cortical networks might optimize information processing. Philos. Trans. A Math. Phys. Eng. Sci. *366*, 329–343.
11. Tagliazucchi, E., Balenzuela, P., Fraiman, D., and Chialvo, D.R. (2012). Criticality in large-scale brain fmri dynamics unveiled by a novel point process analysis. Front. Physiol. *3*, 15.
12. Buzsaki, G. (2006). Rhythms of the Brain (Oxford university press).
13. Buzsáki, G., and Chrobak, J.J. (1995). Temporal structure in spatially organized neuronal ensembles: a role for interneuronal networks. Curr. Opin. Neurobiol. *5*, 504–510.
14. Fries, P., Reynolds, J.H., Rorie, A.E., and Desimone, R. (2001). Modulation of oscillatory neuronal synchronization by selective visual attention. Science *291*, 1560–1563.
15. Fries, P., Womelsdorf, T., Oostenveld, R., and Desimone, R. (2008). The effects of visual stimulation and selective visual attention on rhythmic neuronal synchronization in macaque area v4. J. Neurosci. *28*, 4823–4835.
16. Melloni, L., Molina, C., Pena, M., Torres, D., Singer, W., and Rodriguez, E. (2007). Synchronization of neural activity across cortical areas correlates with conscious perception. J. Neurosci. *27*, 2858–2865.
17. Buzsáki, G. (2005). Theta rhythm of navigation: link between path integration and landmark navigation, episodic and semantic memory. Hippocampus *15*, 827–840.
18. Benchenane, K., Tiesinga, P.H., and Battaglia, F.P. (2011). Oscillations in the prefrontal cortex: a gateway to memory and attention. Curr. Opin. Neurobiol. *21*, 475–485.
19. Klimesch, W., Freunberger, R., Sauseng, P., and Gruber, W. (2008). A short review of slow phase synchronization and memory: evidence for control processes in different memory systems? Brain Res. *1235*, 31–44.
20. Riehle, A., Grün, S., Diesmann, M., and Aertsen, A. (1997). Spike synchronization and rate modulation differentially involved in motor cortical function. Science *278*, 1950–1953.
21. Rossiter, H.E., Davis, E.M., Clark, E.V., Boudrias, M.H., and Ward, N.S. (2014). Beta oscillations reflect changes in motor cortex inhibition in healthy ageing. Neuroimage *91*, 360–365.
22. Başar, E., and Güntekin, B. (2008). A review of brain oscillations in cognitive disorders and the role of neurotransmitters. Brain Res. *1235*, 172–193.
23. Mathalon, D.H., and Sohal, V.S. (2015). Neural oscillations and synchrony in brain dysfunction and neuropsychiatric disorders: it's about time. JAMA Psychiatr. *72*, 840–844.
24. Başar, E., and Güntekin, B. (2013). Review of delta, theta, alpha, beta, and gamma response oscillations in neuropsychiatric disorders. Suppl. Clin. neurophysiol. *62*, 303–341.
25. Engel, A.K., Fries, P., and Singer, W. (2001). Dynamic predictions: oscillations and synchrony in top–down processing. Nat. Rev. Neurosci. *2*, 704–716.
26. Singer, W. (2018). Neuronal oscillations: unavoidable and useful? Eur. J. Neurosci. *48*, 2389–2398.
27. Buzsáki, G., Logothetis, N., and Singer, W. (2013). Scaling brain size, keeping timing: evolutionary preservation of brain rhythms. Neuron *80*, 751–764.
28. Sejnowski, T.J., and Paulsen, O. (2006). Network oscillations: emerging computational principles. J. Neurosci. *26*, 1673–1676.
29. Tiesinga, P., Fellous, J.M., José, J., and Sejnowski, T.J. (2001). Optimal information transfer in synchronized neocortical neurons. Neurocomputing *38–40*, 397–402.
30. Hahn, G., Ponce-Alvarez, A., Deco, G., Aertsen, A., and Kumar, A. (2019). Portraits of communication in neuronal networks. Nat. Rev. Neurosci. *20*, 117–127.
31. Ritz, R., and Sejnowski, T.J. (1997). Synchronous oscillatory activity in sensory systems: new vistas on mechanisms. Curr. Opin. Neurobiol. *7*, 536–546.
32. Ikegaya, Y., Aaron, G., Cossart, R., Aronov, D., Lampl, I., Ferster, D., and Yuste, R. (2004). Synfire chains and cortical songs: temporal modules of cortical activity. Science *304*, 559–564.
33. Abeles, M. (2009). Synfire chains. Scholarpedia *4*, 1441.
34. Fries, P. (2015). Rhythms for cognition: communication through coherence. Neuron *88*, 220–235.
35. Bastos, A.M., Vezoli, J., and Fries, P. (2015). Communication through coherence with inter-areal delays. Curr. Opin. Neurobiol. *31*, 173–180.
36. Tiesinga, P., and Sejnowski, T.J. (2009). Cortical enlightenment: are attentional gamma oscillations driven by ing or ping? Neuron *63*, 727–732.
37. Friston, K. (2002). Functional integration and inference in the brain. Prog. Neurobiol. *68*, 113–143.
38. Deco, G., Tononi, G., Boly, M., and Kringelbach, M.L. (2015). Rethinking segregation and integration: contributions of whole-brain modelling. Nat. Rev. Neurosci. *16*, 430–439.
39. Sporns, O. (2013). Network attributes for segregation and integration in the human brain. Curr. Opin. Neurobiol. *23*, 162–171.
40. Esfahani, Z.G., Gollo, L.L., and Valizadeh, A. (2016). Stimulus-dependent synchronization in delayed-coupled neuronal networks. Sci. Rep. *6*, 23471.
41. Pariz, A., Esfahani, Z.G., Parsi, S.S., Valizadeh, A., Canals, S., and Mirasso, C.R. (2018). High frequency neurons determine effecztive connectivity in neuronal networks. Neuroimage *166*, 349–359.
42. Pariz, A., Fischer, I., Valizadeh, A., and Mirasso, C. (2021). Transmission delays and frequency detuning can regulate information flow between brain regions. PLoS Comput. Biol. *17*, e1008129.
43. Ziaeemehr, A., Zarei, M., Valizadeh, A., and Mirasso, C.R. (2020). Frequency-dependent organization of the brain's functional network through delayed-interactions. Neural Network. *132*, 155–165.
44. Madadi Asl, M., Valizadeh, A., and Tass, P.A. (2023). Decoupling of interacting neuronal populations by time-shifted stimulation through spike-timing-dependent plasticity. PLoS Comput. Biol. *19*, e1010853.
45. Goltsev, A.V., de Abreu, F.V., Dorogovtsev, S.N., and Mendes, J.F.F. (2010). Stochastic cellular automata model of neural networks. Phys. Rev. *81*, 061921.
46. Khaleghi, A., Mohammadi, M.R., Shahi, K., and Motie Nasrabadi, A. (2021). A Neuronal Population Model Based on Cellular Automata to Simulate the Electrical Waves of the Brain, Waves in Random and Complex Media, *1–20*.
47. Lee, K., Goltsev, A., Lopes, M., and Mendes, J. (2013). Neural networks with dynamical synapses: from mixed-mode oscillations and spindles to chaos. AIP Conf. Proc. *1510*, 195–201. American Institute of Physics.
48. Lymperopoulos, I.N. (2021). # stayhome to contain covid-19: Neuro-sir–neurodynamical epidemic modeling of infection patterns in social networks. Expert Syst. Appl. *165*, 113970.

49. Acedo, L., and Moraño, J.A. (2013). Brain oscillations in a random neural network. Math. Comput. Model. *57*, 1768–1772.
50. Buzsáki, G., and Wang, X.J. (2012). Mechanisms of gamma oscillations. Annu. Rev. Neurosci. *35*, 203–225.
51. Geisler, C., Brunel, N., and Wang, X.J. (2005). Contributions of intrinsic membrane dynamics to fast network oscillations with irregular neuronal discharges. J. Neurophysiol. *94*, 4344–4361.
52. Susin, E., and Destexhe, A. (2021). Integration, coincidence detection and resonance in networks of spiking neurons expressing gamma oscillations and asynchronous states. PLoS Comput. Biol. *17*, e1009416.
53. Le Van Quyen, M., Muller, L.E., Telenczuk, B., Halgren, E., Cash, S., Hatsopoulos, N.G., Dehghani, N., and Destexhe, A. (2016). High-frequency oscillations in human and monkey neocortex during the wake–sleep cycle. Proc. Natl. Acad. Sci. USA *113*, 9363–9368.
54. Lisman, J.E., and Jensen, O. (2013). The theta-gamma neural code. Neuron *77*, 1002–1016.
55. Belluscio, M.A., Mizuseki, K., Schmidt, R., Kempter, R., and Buzsáki, G. (2012). Cross-frequency phase–phase coupling between theta and gamma oscillations in the hippocampus. J. Neurosci. *32*, 423–435.
56. Brunel, N., and Wang, X.J. (2003). What determines the frequency of fast network oscillations with irregular neural discharges? i. synaptic dynamics and excitation-inhibition balance. J. Neurophysiol. *90*, 415–430.
57. Wulff, P., Ponomarenko, A.A., Bartos, M., Korotkova, T.M., Fuchs, E.C., Bähner, F., Both, M., Tort, A.B.L., Kopell, N.J., Wisden, W., and Monyer, H. (2009). Hippocampal theta rhythm and its coupling with gamma oscillations require fast inhibition onto parvalbumin-positive interneurons. Proc. Natl. Acad. Sci. USA *106*, 3561–3566.
58. Van Vreeswijk, C., and Sompolinsky, H. (1996). Chaos in neuronal networks with balanced excitatory and inhibitory activity. Science *274*, 1724–1726.
59. Renart, A., De La Rocha, J., Bartho, P., Hollender, L., Parga, N., Reyes, A., and Harris, K.D. (2010). The asynchronous state in cortical circuits. Science *327*, 587–590.
60. Brunel, N. (2000). Dynamics of sparsely connected networks of excitatory and inhibitory spiking neurons. J. Comput. Neurosci. *8*, 183–208.
61. Atallah, B.V., and Scanziani, M. (2009). Instantaneous modulation of gamma oscillation frequency by balancing excitation with inhibition. Neuron *62*, 566–577.
62. Rezaei, H., Aertsen, A., Kumar, A., and Valizadeh, A. (2020). Facilitating the propagation of spiking activity in feedforward networks by including feedback. PLoS Comput. Biol. *16*, e1008033.
63. Barardi, A., Sancristóbal, B., and Garcia-Ojalvo, J. (2014). Phase-coherence transitions and communication in the gamma range between delay-coupled neuronal populations. PLoS Comput. Biol. *10*, e1003723.
64. Pastor-Satorras, R., Castellano, C., Van Mieghem, P., and Vespignani, A. (2015). Epidemic processes in complex networks. Rev. Mod. Phys. *87*, 925–979.
65. Quilichini, P., Sirota, A., and Buzsáki, G. (2010). Intrinsic circuit organization and theta–gamma oscillation dynamics in the entorhinal cortex of the rat. J. Neurosci. *30*, 11128–11142.
66. Penttonen, M., Kamondi, A., Acsády, L., and Buzsáki, G. (1998). Gamma frequency oscillation in the hippocampus of the rat: intracellular analysis *in vivo*. Eur. J. Neurosci. *10*, 718–728.
67. Fernández-Ruiz, A., Oliva, A., Soula, M., Rocha-Almeida, F., Nagy, G.A., Martin-Vazquez, G., and Buzsáki, G. (2021). Gamma rhythm communication between entorhinal cortex and dentate gyrus neuronal assemblies. Science *372*, eabf3119.
68. Sirota, A., and Buzsáki, G. (2005). Interaction between neocortical and hippocampal networks via slow oscillations. Thalamus Relat. Syst. *3*, 245–259.
69. Sanchez-Vives, M.V. (2020). Origin and dynamics of cortical slow oscillations. Curr. Opin. Physiol. *15*, 217–223.
70. Neske, G.T. (2015). The slow oscillation in cortical and thalamic networks: mechanisms and functions. Front. Neural Circ. *9*, 88.
71. Compte, A., Sanchez-Vives, M.V., McCormick, D.A., and Wang, X.J. (2003). Cellular and network mechanisms of slow oscillatory activity (<1 hz) and wave propagations in a cortical network model. J. Neurophysiol. *89*, 2707–2725. https://doi.org/10.1152/jn.00845.2002, pMID: 12612051.
72. Canolty, R.T., and Knight, R.T. (2010). The functional role of cross-frequency coupling. Trends Cognit. Sci. *14*, 506–515.
73. Voytek, B., Canolty, R.T., Shestyuk, A., Crone, N.E., Parvizi, J., and Knight, R.T. (2010). Shifts in gamma phase–amplitude coupling frequency from theta to alpha over posterior cortex during visual tasks. Front. Hum. Neurosci. *4*, 191.
74. Hülsemann, M.J., Naumann, E., and Rasch, B. (2019). Quantification of phase-amplitude coupling in neuronal oscillations: comparison of phase-locking value, mean vector length, modulation index, and generalized-linear-modeling-cross-frequency-coupling. Front. Neurosci. *13*, 573.
75. Kandel, E.R., Schwartz, J.H., Jessell, T.M., Siegelbaum, S., Hudspeth, A.J., Mack, S., et al. (2000). Principles of Neural Science, *volume 4* (McGraw-hill).
76. Gerstner, W., Kistler, W.M., Naud, R., and Paninski, L. (2014). Neuronal Dynamics: From Single Neurons to Networks and Models of Cognition (Cambridge University Press).
77. Hille, B. (1978). Ionic channels in excitable membranes. current problems and biophysical approaches. Biophys. J. *22*, 283–294.
78. Destexhe, A., and Paré, D. (1999). Impact of network activity on the integrative properties of neocortical pyramidal neurons *in vivo*. J. Neurophysiol. *81*, 1531–1547.
79. McCormick, D.A., Wang, Z., and Huguenard, J. (1993). Neurotransmitter control of neocortical neuronal activity and excitability. Cerebr. Cortex *3*, 387–398.
80. Gabbiani, F., Midtgaard, J., and Knöpfel, T. (1994). Synaptic integration in a model of cerebellar granule cells. J. Neurophysiol. *72*, 999–1009.
81. Destexhe, A., Mainen, Z.F., and Sejnowski, T.J. (1994). Synthesis of models for excitable membranes, synaptic transmission and neuromodulation using a common kinetic formalism. J. Comput. Neurosci. *1*, 195–230.
82. Campagnola, L., Seeman, S.C., Chartrand, T., Kim, L., Hoggarth, A., Gamlin, C., Ito, S., Trinh, J., Davoudian, P., Radaelli, C., et al. (2022). Local connectivity and synaptic dynamics in mouse and human neocortex. Science *375*, eabj5861.
83. Sederberg, A., and Nemenman, I. (2020). Randomly connected networks generate emergent selectivity and predict decoding properties of large populations of neurons. PLoS Comput. Biol. *16*, e1007875.
84. Morrison, A., Aertsen, A., and Diesmann, M. (2007). Spike-timing-dependent plasticity in balanced random networks. Neural Comput. *19*, 1437–1467.
85. Gray, R.T., and Robinson, P.A. (2007). Stability and spectra of randomly connected excitatory cortical networks. Neurocomputing *70*, 1000–1012.
86. Börgers, C., and Kopell, N. (2003). Synchronization in networks of excitatory and inhibitory neurons with sparse, random connectivity. Neural Comput. *15*, 509–538.
87. Brunel, N., and Hakim, V. (1999). Fast global oscillations in networks of integrate-and-fire neurons with low firing rates. Neural Comput. *11*, 1621–1671.
88. Roohi, N., and Valizadeh, A. (2022). Role of interaction delays in the synchronization of inhibitory networks. Neural Comput. *34*, 1425–1447.
89. Faci-Lázaro, S., Soriano, J., Mazo, J.J., and Gómez-Gardeñes, J. (2023). Dynamical and topological conditions triggering the spontaneous activation of izhikevich neuronal networks. Chaos, Solit. Fractals *172*, 113547.
90. Park, H.J., and Friston, K. (2013). Structural and functional brain networks: from connections to cognition. Science *342*, 1238411.
91. Watts, D.J., and Strogatz, S.H. (1998). Collective dynamics of 'small-world'networks. Nature *393*, 440–442.
92. Blinowska, K.J., and Kaminski, M. (2013). Functional brain networks: random,"small world" or deterministic? PLoS One *8*, e78763.
93. Hilgetag, C.C., and Goulas, A. (2016). Is the brain really a small-world network? Brain Struct. Funct. *221*, 2361–2366.
94. Vaessen, M.J., Hofman, P.A.M., Tijssen, H.N., Aldenkamp, A.P., Jansen, J.F.A., and Backes, W.H. (2010). The effect and reproducibility of different clinical dti gradient sets on small world brain connectivity measures. Neuroimage *51*, 1106–1116.
95. He, Y., Chen, Z.J., and Evans, A.C. (2007). Small-world anatomical networks in the human brain revealed by cortical thickness from mri. Cerebr. Cortex *17*, 2407–2419.
96. Achard, S., Salvador, R., Whitcher, B., Suckling, J., and Bullmore, E. (2006). A resilient, low-frequency, small-world human brain functional network with highly connected association cortical hubs. J. Neurosci. *26*, 63–72.
97. Bassett, D.S., and Bullmore, E. (2006). Small-world brain networks. Neuroscientist *12*, 512–523.
98. Bassett, D.S., and Bullmore, E.T. (2017). Small-world brain networks revisited. Neuroscientist *23*, 499–516.
99. Steinke, G.K., and Galán, R.F. (2011). Brain rhythms reveal a hierarchical network

organization. PLoS Comput. Biol. *7*, e1002207.

100. Bartos, M., Vida, I., and Jonas, P. (2007). Synaptic mechanisms of synchronized gamma oscillations in inhibitory interneuron networks. Nat. Rev. Neurosci. *8*, 45–56.
101. Maccaferri, G., Roberts, J.D., Szucs, P., Cottingham, C.A., Somogyi, P., and Somogyi, P. (2000). Cell surface domain specific postsynaptic currents evoked by identified gabaergic neurones in rat hippocampus *in vitro*. J. Physiol. *524*, 91–116.
102. Woodin, M.A., Ganguly, K., and Poo, M.m. (2003). Coincident pre-and postsynaptic activity modifies gabaergic synapses by postsynaptic changes in cl- transporter activity. Neuron *39*, 807–820.
103. Izhikevich, E.M. (2004). Which model to use for cortical spiking neurons? IEEE Trans. Neural Network. *15*, 1063–1070.
104. Izhikevich, E.M. (2003). Simple model of spiking neurons. IEEE Trans. Neural Network. *14*, 1569–1572.
105. Rulkov, N.F. (2001). Regularization of synchronized chaotic bursts. Phys. Rev. Lett. *86*, 183–186.
106. Hodgkin, A.L., and Huxley, A.F. (1952). A quantitative description of membrane current and its application to conduction and excitation in nerve. J. Physiol. *117*, 500–544.
107. Hindmarsh, J.L., and Rose, R.M. (1984). A model of neuronal bursting using three coupled first order differential equations. Proc. R. Soc. Lond. B Biol. Sci. *221*, 87–102.
108. Ibarz, B., Casado, J.M., and Sanjuán, M. (2011). Map-based models in neuronal dynamics. Phys. Rep. *501*, 1–74.
109. Daoudal, G., and Debanne, D. (2003). Long-term plasticity of intrinsic excitability: learning rules and mechanisms. Learn. Mem. *10*, 456–465.
110. Shouval, H.Z., Wang, S.S.H., and Wittenberg, G.M. (2010). Spike timing dependent plasticity: a consequence of more fundamental learning rules. Front. Comput. Neurosci. *4*, 19.

STAR★METHODS

KEY RESOURCES TABLE

REAGENT or RESOURCE	SOURCE	IDENTIFIER
Software and algorithms		
DEV C++ Version 6.3	Repository	https://github.com/Embarcadero/Dev-Cpp
Python	Python Software Foundation	https://www.python.org
Jupyter Notebook	Jupyter Website	https://jupyter.org/
Deposited data		
Resource website for the deposited codes	Zenodo	https://doi.org/10.5281/zenodo.10688712
Resource website for the output of the C++ codes as data for analysis	Zenodo	https://doi.org/10.5281/zenodo.10688769

RESOURCE AVAILABILITY

Lead contact

Further information and requests for resources and reagents should be directed to and will be fulfilled by the lead contact, Alireza Valizadeh (valizade@iasbs.ac.ir).

Materials availability

This study did not generate new unique reagents.

Data and code availability

- The output of codes as data have been deposited at Zenodo and are publicly available as of the date of publication. DOIs are listed in the key resources table.
- All original codes has been deposited at Zenodo and are publicly available as of the date of publication. DOIs are listed in the key resources table.
- Any additional information required to reanalyze the data reported in this paper is available from the lead contact upon request.

METHOD DETAILS

We used C++ for all numerical simulations. The network was composed of $N = 5000$ neurons that 80 percent were excitatory. To create the ER network, where nodes are connected randomly, we fixed the connection probability p which sets the mean value of incoming/outgoing synapses such that $\langle k \rangle = (N-1)p$. To reproduce the ER network with different connection probability in each block of the adjacency matrix, we changed the connection probability for each block separately. For the results shown in Figure S4, we set $p = 0.05$ for block $\mathcal{E} \rightarrow \mathcal{E}$ while setting $p = 0.1$ for the other blocks. But, to maintain the same mean input as in Figure 3 for a more accurate comparison, we set $A_{ij} = 2$ for nodes $1 \leq i, j \leq N_{\mathcal{E}}$ $(i \neq j)$ which were linked, such that the synaptic input among excitatory neurons was twice stronger than that of $\mathcal{E}$ to $\mathcal{I}$ neurons. For a k-regular structure, we first fixed the number of in-going links in a diagonal block $\alpha \rightarrow \alpha$ for each node as $k_{\alpha \rightarrow \alpha}$, as well as the exact number of out-going links in blocks $\alpha \rightarrow \beta$ $(\alpha, \beta \in \{\mathcal{E}, \mathcal{I}\})$, namely $k_{\alpha \rightarrow \beta}$, based on the desired degree. Then for diagonal blocks, putting the excitatory nodes on a circle as well as inhibitory nodes on another circle, each node was connected to its $k_{\alpha \rightarrow \alpha}/2$ nearest neighbors on each side, and also to the nodes directly opposite. The same was applied for connecting the nodes of opposite types regarding $k_{\alpha \rightarrow \beta}/2$ for the anti diagonal blocks. It is worthwhile to mention that since the number of excitatory nodes was four times of inhibitory ones, we set $k_{\mathcal{I} \rightarrow \mathcal{E}} = 4k_{\mathcal{E} \rightarrow \mathcal{I}}$ to obtain a balanced structure. A schematic representation of the adjacency matrix of such a network, consisting four k-regular blocks of $\mathcal{E} \rightarrow \mathcal{E}$, $\mathcal{E} \rightarrow \mathcal{I}$, $\mathcal{I} \rightarrow \mathcal{E}$, and $\mathcal{I} \rightarrow \mathcal{I}$, is shown in Figure S5A. Certainly, all nodes have uniform incoming excitatory and inhibitory links, as well as identical outgoing links of type E and I, respectively for $\mathcal{E}$ and $\mathcal{I}$ nodes. Then, we proceeded to modify the structure of block $\mathcal{E} \rightarrow \mathcal{E}$ to resemble a small-world network by adding some new links randomly (see Figure S5B). For a balanced structure, it was important to set parameters carefully; e.g. for a k-regular network with a small-world excitatory block and $N = 5000$, $\langle k_{in}^{i,\mathbb{E}} \rangle \approx 400$, $\langle k_{in}^{i,\mathbb{I}} \rangle \approx 100$, we set $k_{\mathcal{E} \rightarrow \mathcal{E}} = 330$, $k_{\mathcal{I} \rightarrow \mathcal{I}} = 100$, $k_{\mathcal{E} \rightarrow \mathcal{I}} = 100$, and $k_{\mathcal{I} \rightarrow \mathcal{E}} = 400$, then new random excitatory links were created in block $\mathcal{E} \rightarrow \mathcal{E}$ with a probability of 0.02. We denoted the state of node i at time t with $\pi_i(t) \in \{0, 1\}$ such that $\pi_i = 1$ (0) for a firing (resting) neuron. Also, in the implementation code, the state of a type $\alpha \in \{\mathbb{E}, \mathbb{I}\}$ link from node i to j was indicated with a counter $C_{ji}(t)$ at time t, such that $0 < C_{ji} \leq \delta_\alpha$ if the link was active and otherwise $C_{ji} = 0$. Based on the external input, respectively $\eta N_{\mathcal{E}}$ excitatory and $\eta N_{\mathcal{I}}$ inhibitory neurons became active at $t = 0$ randomly. Increasing time, the state of links was updated according to the pre-synaptic nodes state or links counter as follows. If $C_{ji}(t-1) = 0$ and $\pi_i(t-1) = 1$, then $C_{ji}(t) = 1$. In the case that $1 \leq C_{ji}(t-1) < \delta_\alpha$, we set $C_{ji}(t) = C_{ji}(t-1) + 1$, and links with $C_{ji}(t-1) = \delta_\alpha$ became inactive such that $C_{ji}(t) = 0$. Once

updating links counters, the input current of nodes was obtained based on active in-going links. If the total input of node *i* was more than the threshold, then $\pi_i(t) = 1$. We also made some nodes active randomly as a result of external input based on the η value. Then, the density of active excitatory and inhibitory neurons at time *t* would be $\rho_{\mathcal{E}}(t) = \frac{1}{N}\sum_{i=1}^{N_{\mathcal{E}}} \pi_i(t)$ and $\rho_{\mathcal{I}}(t) = \frac{1}{N}\sum_{i=1}^{N_{\mathcal{I}}} \pi_i(t)$, respectively. It was also possible to obtain the density of active links, i.e. $\varphi_{\mathbb{E}}$ and $\varphi_{\mathbb{I}}$, by counting links whose counter value was not zero. The code was run for at least $t_{max} = 25000$ time steps. The main output of the simulation was a $t_{max}\times 3$ matrix where columns denoted the time, $\rho_{\mathcal{E}}$, and $\rho_{\mathcal{I}}$, respectively from left to right. To replicate the results for an exponential decay for the synaptic input shown in Figures S6 and S7, while we regarded δ_α initially as the activation time steps of an α type synapse (Figure 1D), here we considered δ_α as *the decay time constant* of active links (see Figures S6A–S6C). We assumed that when a synapse became active at time $t = 0$, the post-synaptic neuron received an amount of 1 and -4 units of input on that time through excitatory and inhibitory links, respectively. Then, for the subsequent time steps, the synaptic input decayed as $\exp^{-t/\delta_{\mathbb{E}}}$ and $-4\exp^{-t/\delta_{\mathbb{I}}}$. Here *t* was a discrete value corresponding to the time step ranged between zero and a cut-off value which we set such that the excitatory input current became close to zero. Finally, we imported the output into Python to analyze the power spectrum of the network activity. Using Numpy, we calculated the population frequency by applying fast Fourier transform (FFT) to ρ and recording the frequency with the highest spectral power. Additionally, we analyzed the characteristics of activity cycles at different states by determining the start point, end point, and maximum value of each cycle. As shown in Figure 3C, we defined the width of each activity as the time interval between two consecutive start and end points, while the amplitude was identified as the maximum value of ρ within this interval. Additionally, we calculated the burst period as the time interval between the start and end points of the first and last activity cycles within a burst. The silence periods were determined as the time interval between the end and start points of two adjacent bursts. We also utilized the Scipy library to examine the phase amplitude coupling of the intermittent state. To start, we used functions signal.firwin and signal.filtfilt to obtain high- and slow-frequency oscillations in the frequency ranges of interest (see Figure 6B). Then, SOP and FOA were extracted from the Hilbert transformation of slow and fast oscillations, respectively (see ref.[74]).